

Size and promoter effects on iron nanoparticles confined in carbon nanotubes and their catalytic performance in light olefin synthesis from syngas

Bang Gu, Cheng Zhou, Shun He, Simona Moldovan, Petr Chernavskii, Vitaly Ordomsky, Andrei Khodakov

▶ **To cite this version:**

Bang Gu, Cheng Zhou, Shun He, Simona Moldovan, Petr Chernavskii, et al.. Size and promoter effects on iron nanoparticles confined in carbon nanotubes and their catalytic performance in light olefin synthesis from syngas. Catalysis Today, 2019, 357, pp.203-213. 10.1016/j.cattod.2019.05.054 . hal-02169585

HAL Id: hal-02169585

https://normandie-univ.hal.science/hal-02169585

Submitted on 24 Oct 2022

HAL is a multi-disciplinary open access archive for the deposit and dissemination of scientific research documents, whether they are published or not. The documents may come from teaching and research institutions in France or abroad, or from public or private research centers.

L'archive ouverte pluridisciplinaire **HAL**, est destinée au dépôt et à la diffusion de documents scientifiques de niveau recherche, publiés ou non, émanant des établissements d'enseignement et de recherche français ou étrangers, des laboratoires publics ou privés.



Distributed under a Creative Commons Attribution - NonCommercial| 4.0 International License

Version of Record: https://www.sciencedirect.com/science/article/pii/S0920586118313944
Manuscript_8ac9db8e7f49b4831e2c170d93cd42ba

Revision, March 16th 2019

Size and Promoter Effects on Iron Nanoparticles Confined in Carbon Nanotubes and their Catalytic Performance in Light Olefin Synthesis from Syngas

Bang Gu[a], Cheng Zhou[b], Shun He[b], Simona Moldovan[c], Petr A. Chernavskii[d], Vitaly V. Ordomsky [a,*] and Andrei Y. Khodakov[a,*]

[a]*Univ. Lille, CNRS, Centrale Lille, ENSCL, Univ. Artois, UMR 8181 – UCCS – Unité de Catalyse et Chimie du Solide, F-59000 Lille, France.*

[b]*Collaborative Innovation Center of Chemistry for Energy Materials, State Key Laboratory of Physical Chemistry of Solid Surfaces, Xiamen University, 361000 Xiamen, China.*

[c] *Groupe de Physique des Matériaux, CNRS, Université Normandie & INSA Rouen Avenue de l'Université - BP12, 76801 St Etienne du Rouvray.*

[d] *Department of Chemistry, Moscow State University, 119992 Moscow, Russia.*

Corresponding authors:

vitaly.ordomsky@univ-lille.fr and andrei.khodakov@univ-lille.fr

© 2019 published by Elsevier. This manuscript is made available under the CC BY NC user license
https://creativecommons.org/licenses/by-nc/4.0/

Abstract

Light olefins are important products of high temperature Fischer-Tropsch synthesis over iron catalysts. In this paper, we found that the catalytic performance of iron catalysts was strongly affected by iron nanoparticle size, their encapsulation inside of carbon nanotubes and promotion with bismuth or lead. The presence of promoters and iron nanoparticle confinement leads to a major increase in the reaction rate. A gradual increase in the TOF numbers with the increase in the iron nanoparticle sizes from 2.5 to 12 nm was observed at both 1 and 10 bar over the carbon nanotubes containing encapsulated monometallic or Bi- or Pb-promoted iron nanoparticles. The size of monometallic iron nanoparticles encapsulated in carbon nanotubes does not show any noticeable effect on the light olefin selectivity, while in the Bi- and Pb-promoted catalysts, the light olefin selectivity was higher over smaller encapsulated iron nanoparticles and decreased with the increase in the nanoparticle size. The stability of iron nanoparticles versus sintering was also improved by the encapsulation.

Keywords: Fischer-Tropsch; Particles size; Confinement; Lower olefins; Iron; Promoter

1. Introduction

Light olefins (ethylene, propylene and butene) are key building-block chemicals, which are widely used in the chemical industry[1-3]. Currently, light olefins are primarily produced via stream cracking of naphtha or methanol-to-olefins (MTO) process, while ethylene is also manufactured from ethane cracking [4]. The growing demand for light olefins and depletion of oil reserves have stimulated development of processes for light olefin synthesis from syngas, which might be produced from alternative feedstocks such as methane, biomass, coal or organic and plastic wastes. Fischer-Tropsch (FT) synthesis produces hydrocarbons from syngas. High temperature FT synthesis (300- 350 °C) is mainly used for production of gasoline and light olefins [5, 6]. FT synthesis is one of the most efficient ways to convert syngas directly into light olefins [7-9]. In the olefin synthesis from syngas, Fe-based catalysts can be the catalysts of choice, because of their low cost, high selectivity towards olefins and flexibility relative to the use of syngas with different H_2/CO ratios [4, 10-12].

FT synthesis is often considered as a structure sensitive reaction and particle size may have noticeable effects both on the activity and selectivity [13-16]. The particle size effects over cobalt [17-20] and ruthenium-based [21-23] catalysts in low temperature FT synthesis have been addressed in numerous publications. The optimum cobalt and ruthenium size was found to be about 6-8 nm. The increase in the size of metal

nanoparticles above 8 nm leads to lower overall activity, while the metal particles with the sizes smaller than 6 nm demonstrate both lower intrinsic activity (Turnover Frequency, TOF) and lower selectivity toward the C_{5+} hydrocarbons. The particle size effects over iron-based FT catalysts can be rather complex, because of simultaneous presence of different iron phases and catalyst deactivation.

Previous reports suggest that the selectivities to methane and lighter hydrocarbons increase, when iron nanoparticles in supported catalysts are getting smaller than 6–9 nm [24]. TOF increases with the increase in the particle sizes from 2.4 to 6.2 nm and it remains almost constant up to the particle size of 11.5 nm. The stability of iron particles in silica-supported catalysts was previously studied [25, 26] in the nanoscale range (9–20 nm). On the one hand, smaller iron-carbide nanoparticles were found more difficult to obtain by carbidisation of iron oxides and on the other hand, they were less stable than larger particles**.**

The iron particle size effects on the catalytic performance in FT synthesis might be influenced by catalyst promotion and metal-support interactions. In the oxide-supported catalysts, the active metal can react with a support and form barely reducible aluminates or silicates and thus, hinder formation and reduce the stability of active iron carbide phase. The metal support interactions are usually weaker in the carbon-supported catalysts. De Jong [27, 28] *et al* examined the influence of iron carbide particle size in the promoted and unpromoted carbon nanofiber supported iron catalysts on the syngas conversion to light olefins. The TOF numbers of unpromoted catalysts increased 6-8 times with particle size decreasing from 7 to 2 nm, while the

selectivities to methane or light olefins were found independent on the particle size [27]. The iron catalysts promoted with sodium and sulphur showed similar variation of TOF as a function of particle size. The increase in TOF with decrease in iron particle size in the promoted catalysts was principally due to higher yield of methane over the smallest particles. Recently, we have discovered strong promoting effects of Bi and Pb on the catalytic performance of Fe catalysts in FT synthesis [29, 30]. The effects have been attributed to the enhanced C-O dissociation on the surface of iron carbide nanoparticles in the presence of Bi and Pb, which significantly increases catalyst activity and selectivity to light olefins.

A number of previous works suggest important influence of iron nanoparticles confinement in carbon nanotubes (CNT) on the electronic structure, catalytic performance and stability of iron FT catalysts [31-33]. Bao [34] *et al* found that iron nanoparticles confined in CNT exhibited better reducibility, carbidisation and much higher activity in FT synthesis compared to the unconfined counterparts, while the selectivity to light olefins was not much affected by the confinement [35, 36]. Higher reaction rate was principally attributed to higher extent of iron carbidisation inside CNTs. The encapsulation of nanoparticles also protects them from sintering [37]. Analysis of the electron distribution in CNT using DFT [38] showed that the curvature of the CNT induced a significant electron disparity. More electrons were distributed on the exterior surface of the CNT. This led to stronger bonding of iron species with the outside CNT surface than those located the inside CNT walls. These

electronic effects might result in different catalytic activity of iron inside and outside CNT.

The present work addresses the size effects of iron nanoparticles encapsulated inside of CNT on syngas conversion to light olefins. To the best of our knowledge, there have been no studies about the effect of the size of iron nanoparticles confined inside CNT on their properties and catalytic performance. Both monometallic iron catalysts and catalysts promoted with bismuth and lead have been studied. The syngas conversion to lower olefins has been performed at both high and atmospheric pressures at the temperatures typical of high temperature FT synthesis.

2. Experimental

2.1 CNT pre-treatment

Prior to the deposition of iron and promoters, the CNTs were pre-treated according to previous literature [34]. CNTs (Iolitec nanomaterial, 95%, inter diameter 5-12 nm, outer diameter 10-20 nm) were exposed to boiling concentrated nitric acid in order to open the tube channels, to remove contaminations and to make CNT hydrophilic. Typically, 3.0 g of CNT were pre-treated in concentrated HNO_3 (68%, 210 mL) during 14 h under reflux at 140 ºC. Then the samples were filtered, washed with distilled water until pH = 7 and dried at 100 ºC overnight. CNT with closed tube channels were pre-treated under milder condition (34 wt. % HNO_3 for 6h at 110ºC).

2.2 Catalyst preparation

The encapsulated iron catalysts were prepared by incipient wetness impregnation of CNT support with aqueous solutions of iron nitrate ($Fe(NO_3)_3 \cdot 9H_2O$, Sigma-Aldrich). The amount of iron in the impregnating solutions was calculated in order to obtain 10 wt. % iron in the final catalysts. Lead nitrate ($Pb(NO_3)_2$, Sigma-Aldrich) and bismuth nitrate ($Bi(NO_3)_3 \cdot 5H_2O$, Sigma-Aldrich) were used for preparation of the Bi- and Pb-promoted iron catalysts by co-impregnation. The aqueous solutions were drawn into the CNT channels by capillary forces assisted by ultrasonic treatment and stirring. The molar ratios of Fe/Pb and Fe/Bi were 100/2. After the impregnation, the samples were dried in an oven at 80 °C for 12 h followed by thermal treatment for 4 h under a flow of nitrogen (50 mL/min). The temperature of thermal treatment was varied from 300 to 600 °C in order to obtain different iron particle size. The calcined catalysts are labelled as Fe*M*/CNT-in-*T*, where "*M*" represents the promoters (Bi or Pb), "in" represents iron inside the CNT tubes and "*T*" stands for thermal treatment temperature. For comparison, the Fe/AC and Fe/CNT-out catalysts, where "out" indicates iron particles located outside the tubes, were prepared by the same procedure. The temperature of thermal treatment in the N_2 flow for those 2 samples is 400 °C; the duration is 4h. The iron content in these two catalysts is 10 wt.%.

2.3. Catalyst characterization

Low temperature N_2 physisorption measurements were carried out using a Micromeritics Tristar 3020 Surface Area and Porosimetry analyzer. The samples were

degassed at 200 ºC for 2 h to remove water before N_2 adsorption. The N_2 adsorption-desorption isotherms were measured at -196°C.

The X-ray diffraction patterns (XRD) were recorded using a Siemens D5000 diffractometer. The measurement conditions were: Cu(Kα) (λ = 0.15418 nm), tube pressure 40 kv, tube current 30 mA, and scanning rate 0.02° s^{-1}. The phase composition analysis of the samples was performed by comparing the XRD Standards Database of the Joint Committee on Powder Diffraction Standards (JCPDS). The average crystallite size of iron oxides (Fe_2O_3) was evaluated by the Scherrer equation [39] using the diffraction peak of Fe_2O_3 at 2θ of 30.2º.

Quantitative elemental analyses were performed by inductively coupled plasma-optic emission spectroscopy 720-ES ICP-OES (Agilent) with axially viewing and simultaneous CCD detection. The quantitative determination of metal content in the catalysts was based on the analysis of standard solutions. The ICP ExpertTM software (version 2.0.4) provided metal concentration in the samples. The minimum detection limitation is 0.1 ppm and the accuracy is better than 5%.

The H_2 temperature-programmed reduction (H_2-TPR) experiments were carried out by the AutoChem II 2920 apparatus (Micromeritics) using 0.10 g of the sample in a flow of H_2/Ar (5 vol. % H_2) stream (50 ml/min). The temperature was increased from room temperature to 900 °C at the rate of 10 °C/min.

The TEM (Transmission Electron Microscopy) analyses were carried out on a Phillips FEI G2 30 high resolution transmission electron microscope with an accelerating voltage of 300 KV. The sample was prepared by dispersing in an ethanol

solution. After 1 h of ultrasonication, the sample slurry was dropped onto a 400-mesh carbon film copper mesh, and dried under an infrared lamp to test. High angle annular dark field (HAADF)-scanning transmission electron microscopy (STEM) imaging, and energy dispersive X-ray spectroscopy (EDX) of the calcined analysis were performed on a Jeol-ARM200 transmission electron microscope, operated at 200 kV and scanning speed 20 μs/px for imaging and 0.05 μs/px for EDX. More than 200 iron particles were counted to estimate the iron particles size distribution and average iron particle size.

In-situ magnetic characterization has been performed using a Föner vibrating-sample magnetometer. 1 mg of pure metallic Fe was used for the calibration before each experiment. 10 mg of the fresh catalysts was heated to 200 °C with the ramping rate 6.6 °C/min in the flow of CO or syngas (15 ml/min) and then sequentially heated to 350 °C (4.7 °C/min) for 2 h in CO or syngas. After activation, the sample was cooled to RT in the atmosphere of CO or syngas with the saturation magnetization curve recorded by the magnetometer.

2.4. Catalytic tests

The catalytic tests in FT synthesis were performed in a fixed-bed reactor (8 mm inner diameter). Typically, 0.1 g of fresh catalyst with the particle size of 100-150 μm was loaded in the reactor and then reduced in the CO gas flow (50 ml/min, atmospheric pressure) at 350 ^{o}C with a heating rate of 2 ^{o}C/min for 10 h before the reaction. After the reactor was cooled down to 180 ^{o}C, a syngas with the H_2/CO ratio of 1/1 and under pressure of 10 or 1 bar was introduced into the reactor. Nitrogen with

a fixed flow rate of 1 ml/min in the syngas was used as an internal standard for the calculation of CO conversion. After the pressure and gas flow rate stable, the temperature was raised with the ramping rate of 1 ^{o}C/min to the desired reaction temperature (350 ^{o}C). The absence of mass transport resistances was checked by Weisz-Prater Criterion (N_{W-P}) for internal diffusion [40-42].

$$N_{W-P} = \frac{R r_p^{\,2}}{D_{eff} C_s} \leq 0.3$$

where R = observed reaction rate (mol_{CO} g^{-1} s^{-1}), r_p= catalyst particle radius (m), D_{eff} = effective diffusivity (cm^2 s^{-1}), Cs = gas concentration of CO at the external surface of the catalyst (mol cm^{-3}). We considered a total gas flow rate of 57 ml min^{-1} with ~ 60 % CO conversion and a catalyst particle size of 0.10 - 0.15 mm. The pressure was 10 bar and the reaction rate was calculated from the measured FTY of $6.1*10^{-4}$ mol_{CO} $g_{Fe}^{-1}s^{-1}$. Cs and D_{eff} are calculated according to the literature [43] with the values of $4.9*10^{-5}$ and 0.0229 cm^2 s^{-1}, respectively. The N_{w-p} value is calculated to be 2×10^{-3}, which is much lower than 0.3.

The reaction feed gas and gaseous products were analysed online using a gas chromatograph (Bruker GC-450), which was equipped with a thermal conductivity (TCD) and a flame ionization (FID) detectors. The packed CTR-1 column is connected to the TCD detector for separation of N_2, CO, CO_2, and CH_4. The Rt-Q PLOT capillary column is connected to the FID detector for analysis of hydrocarbons and oxygenates. The liquid products were collected in a cold trap and analysed by gas chromatography. The selectivities were calculated on carbon basis. The CO_2 free hydrocarbon selectivities were calculated considering only hydrocarbon production in

FT synthesis. The carbon balance was better than 90%.

The iron time yields (FTY) were expressed as moles of CO converted per gram of total iron per second. Apparent turnover frequency (TOF) was calculated according with previous literature [16, 27] using the bulk density of Fe_5C_2 (ρ = 7.57 g mL^{-1}) and assuming the surface density of 14 Fe atoms nm^{-2}.

3. Results and discussion

3.1 Catalyst structure

Tables 1 and **2** show textural properties and elemental composition of the CNTs supported monometallic and Bi- or Pb-promoted iron nanoparticles exposed to different temperatures. The impregnation of CNTs with iron decreases the surface area, total pore volume and mesopore diameter. Interestingly, the pore volume is decreased after introduction of iron from 0.83 cm^3/g to about 0.50 cm^3/g. This suggests that some iron particles are located inside of the CNT tubes. Localization of iron nanoparticles inside CNT leads to the decrease in the pore volume and partial blocking of the tubes. The presence of the Bi and Pb promoters, in addition to iron, results in only very small effect on the texture of CNT catalysts. Indeed, the BET surface area and pore volume are almost not affected by the presence of the promoters.

The elemental analysis (**Tables 1** and **2**) shows that all monometallic iron catalysts supported by carbon nanotube treated in nitrogen at different temperatures contain

around 10 wt.% iron. Iron content in the promoted catalysts was also close to10 wt. %, while the contents of bismuth and lead were respectively ~0.85 wt.% and ~0.90 wt.%.

Figure 1a displays XRD profiles of the CNT containing confined monometallic and promoted iron nanoparticles treated in nitrogen at different temperatures. The peaks at 26.3° and 43.8° are attributed to the (002) and (101) reflections of the CNT supports [44]. The diffraction lines at 2θ of 30.2° and 35.6° can be assigned to the hematite phase (Fe_2O_3, JCPDS13-0534), while the diffraction lines at 2θ of 35.8°,43.5° and 53.9° can be ascribed to the magnetite phase (Fe_3O_4, JCPDS 75-0449). The iron oxide peaks become sharper with higher pre-treatment temperature probably due to increase in the iron oxide particle sizes. The iron crystallite sizes have been evaluated from the Scherrer equation (**Table 1**). The iron crystallite size increases from 2.6-2.8 nm for the iron catalysts treated at 300 °C to 11-12 nm for the catalysts treated in nitrogen at 600 °C. Note that the promotion with Bi and Pb does not noticeably affect the iron oxide particle size (**Table 2**). Our previous studies [29, 30] also showed insignificant effect of the bismuth and lead promotions on iron dispersion and iron oxide nanoparticle sizes in the SiO_2 and CNT supported iron catalysts. The confined iron catalysts contain smaller particles compared with the Fe/AC iron catalysts supported on active carbon (**Figure S1** and **Table S1, SI**). The difference is more pronounced, when the Fe/AC catalysts were calcined at higher temperatures. It is interesting to note that maximum size of encapsulated metal oxide nanoparticles corresponds to the internal diameter of CNT (14.4 nm). This is consistent with

localization of iron oxide nanoparticles inside the CNT and suggests that the growth of iron oxide crystallites inside the CNT could be limited by the CNT diameter.

The TEM images and particle size distribution of the encapsulated monometallic iron catalysts with different calcination temperatures are shown in **Figures 2** and **3.** It is clear that most of the particles are located inside of the nanotubes. This clearly confirms confinement of iron nanoparticles inside the CNT in the prepared catalysts. The iron oxides particles size increases from 2.8 nm to 11.4 nm with increase in the pre-treatment temperature. The iron oxide nanoparticle size measured by TEM is consistent with XRD results. The TEM images and particle size distribution for the Bi- or Pb-promoted iron catalysts at different calcination temperature are shown in **Figures 4, S2** and **S3, Supporting Information (SI)**. Importantly, in the catalysts, iron oxide nanoparticles are selectively confined inside the CNT. Similar effects of the pre-treatment temperature on the iron oxide particle sizes were observed with and without promoters (**Table 1** and **2**). Thus, the characterisation suggests that the promoter does not affect the size of metal nanoparticles.

STEM-HAADF and STEM-EDS analysis have been performed in order to further confirm localization of iron and promoters in CNT (**Figure 5**). Bi is a heavier metal compared to iron. In the STEM-HAADF images, the Bi species correspond to brighter spots compared to iron. STEM-EDX indicates that Bi is uniformly distributed on the surface of Fe nanoparticles. These results are similar to our previous data obtained for iron-supported catalysts promoted by Bi and Pb over the SiO_2 and CNT supports. Because of low melting points, metallic bismuth and lead migrate to the iron

nanoparticles and form core-shell structures during catalyst activation and reaction. These core-shell structures were identified by the EDS analysis [29, 30].

The reducibility of iron oxide nanoparticles encapsulated inside CNT was investigated by H_2-TPR**.** **Figure 6a** shows the TPR profiles of the monometallic Fe/CNT-in catalysts with encapsulated iron oxide nanoparticles of different sizes. The TPR profiles exhibit three main broad peaks located at around 390, 450 and 650 ºC. According to the literature [33, 45, 46], the first peak can be assigned to the reduction of Fe_2O_3 to Fe_3O_4, the second peak to the reduction of Fe_3O_4 to FeO and the third peak to the reduction of FeO to metallic Fe. Note that some hydrogen consumption can due to the reductive removal of carboxyl and other oxygen-containing groups from the surface of CNT during the treatment in hydrogen. The small and broad peaks located at 700-800 ºC can be caused by gasification of the CNT support [13]. Because of low amounts of bismuth and lead, no TPR peaks could be assigned to the reduction of the promoters**.** The Fe/CNT-out catalyst containing iron nanoparticles outside the CNT channels has been used as a reference (**Figure 6a**). Interestingly, the encapsulated iron catalysts can be reduced at lower temperatures compared with the Fe/CNT-out catalyst. This suggests that the confinement increases the iron reducibility in agreement with the works of Bao' group [34]. Moreover, as the iron particle size inside the CNT channels increases, the intensity of reduction peaks decreases and they slightly shift to lower temperatures. Similar effect also has been discovered by Park [24] over alumina supported iron catalysts with different crystal sizes. This effect might be explained by easier reducibility of larger iron oxide

nanoparticles. Easier reducibility of larger metal oxide nanoparticles compared to smaller counterparts has been previously observed in numerous publications [25, 47, 48].

Introduction of the Bi and Pb promoters to the iron catalysts does not change significantly the relative position of the TPR peaks but shifts their maximums by approximately 10 ºC to lower temperatures (**Figure 6b, Table 2**). This indicates that promotion of the CNT containing confined iron nanoparticles enhances iron reducibility. Similar effects were also observed recently for the silica and CNT supported FeBi and FePb catalysts [29, 30]. Note that previously prepared promoted iron catalysts supported over CNT contained iron nanoparticles only outside the CNT [30]. Thus, Bi and Pb also promote iron reducibility by increasing total hydrogen consumption and decreasing the reduction temperature in both confined and non-confined systems.

Iron carbide has been considered active phase for iron-based Fischer-Tropsch catalysts. Iron carbide can be formed during activation in the presence of CO prior to the reaction. The XRD for the used catalysts shows a broad peak, which corresponds to the mixture of different iron carbide phase (χ-Fe_5C_2, ε-$Fe_{2.2}C$, Fe_3C, or Fe_7C_3, **Figure S4**, **SI**). Similar results were obtained for the Fe/CNT and FeBi/CNT catalysts [30]. In order to identify iron carbide phase, the *in-situ* magnetic measurements [49, 50] were conducted in the flow of CO or syngas at different temperatures (**Figure S5, SI**). The two examined Fe/CNT-in and FeBi/CNT-in catalysts present a similar shape of thermomagnetic curves with the Curie temperature of ~ 250ºC. According to our

previous report [30], the main iron carbide phase has been identified as χ-Fe_5C_2 in the catalysts exposed to the flow of CO or syngas. Interestingly, the iron carbide concentration was higher in the Bi promoted iron catalyst.

3.2 Catalytic results

The catalytic data are shown in **Tables 3** and **4** and in **Figures 7-11, S6** and **S7, SI.** High temperature FT synthesis yields methane, C_2-C_4 hydrocarbons, C_{5+} hydrocarbons, CO_2 and water. The CNT with encapsulated monometallic and Bi-or Pb-promoted iron nanoparticles with different sizes have been tested in a fix-bed reactor both at high (10 bar) and atmospheric pressure at T = 350 ^oC and H_2/CO = 1/1. For comparison, Fe/CNT-out and Fe/AC have been also tested under the same conditions (**Table 3**). The activity of Fe/CNT-out is 1.5 times higher than for the Fe/AC catalyst. Note however that the confined catalysts present 2-4 times higher reaction rate compared with the Fe/AC catalyst.

The selectivity to light olefins and C_{5+} hydrocarbons follows the sequence: Fe/AC< Fe/CNT-out< Fe/CNT-in, whereas the methane selectivity shows the opposite trend. These results are consistent with earlier data of Bao's group [34]. The effect of confinement on the chain growth probability is relatively small, while the ratio of olefins to paraffins increases in the confined catalysts. Stronger interaction of CO with the CNT internal surface [51, 52] can lead to lower H_2/CO ratio inside the CNT and thus decreases the secondary olefin hydrogenation. **Figure 7** displays CO conversion and product selectivities for the CNT containing encapsulated iron

monometallic nanoparticles as functions of iron particle sizes. At high pressure and at GHSV = 17 L/g.h, carbon monoxide conversion over monometallic iron catalysts increases from 18 to 34 % with the increase in the encapsulated iron particle sizes from 2.8 to 6 nm. Interestingly, further increase in the iron nanoparticle sizes leads to the decrease in the CO conversion. Note that the FT reaction rates were much lower at atmospheric pressure compared to the tests conducted at 10 bar. The selectivities to methane and light olefins over the iron unpromoted nanoparticles at the 10 bar test were about 28 % and 37 %, respectively. Interestingly, these two values do not change much with increasing iron particles size. In order to compare the reaction selectivities, the carbon monoxide conversion was adjusted to the 40-50% level by varying GHSV. Relevant selectivity data are presented in **Figure 8.** The increase in the size of iron nanoparticles encapsulated in CNT does not significantly affect the olefin selectivity and olefin to paraffin ratio over the unpromoted iron catalysts. The selectivity to the C_{5+} hydrocarbons increases from 16.1 to 19.9% with the iron particles size increase from 2.8 nm to 6.0 nm and then stabilises. Further particle size increase from 6.0 nm to 11.4 nm does not affect the reaction selectivity [24]. For comparison, iron catalysts supported over active carbon with different particles size (Fe/AC) has been tested in FT synthesis (**Table S1, SI**). Similar trend has been found as for the Fe/CNT-in-T catalysts. Thus, we found that over the unpromoted, confined or unconfined iron catalysts, particle size does not noticeable affect the light olefin selectivity. These results are consistent with the data of De Jong [27] who also

observed similar selectivity to methane and lower olefins is over the iron particles of different sizes in FT reaction over unpromoted iron catalysts.

Different to the unpromoted iron catalysts, the size of Bi-promoted and encapsulated iron particles has strong effects both on the activity and selectivity (**Figure 8**). The presence of the promoters significantly increases the FT reaction rate. The FeBi/CNT-in catalyst shows more than 2 times higher FTY in comparison with the Fe/CNT-in catalyst at the pressure of 10 bar (**Figures 9** and **10, S6, SI, Table 4**). The reaction selectivity shifts to the C_2-C_4 light hydrocarbons compared to the monometallic Fe/CNT-in catalyst. The methane selectivity decreases from ~29 % to ~ 25 % and C_{5+} decreases from ~ 20 % to ~12%. In addition, the selectivity of lower olefins increases from ~ 35 % to ~ 45%. The selectivity to CO_2 also increases over the FeBi/CNT-in catalysts compared with the monometallic Fe/CNT-in counterparts. The effect can be due to easing CO dissociation on iron carbide via oxygen removal from iron carbide by scavenging with the promoters [29, 30]. The catalytic activity in the presence of the promoters increases with increase in iron nanoparticle size until 6 nm and then decreases at the larger iron nanoparticle sizes. More importantly, this promotion effect is also significant even under atmospheric pressure with the 2-3 times increase in the FTY in comparison with the non-promoted catalysts. Compared with the Bi promoted iron catalysts, the FePb/CNT-in catalysts present even much more significant increase in FTY (~2.5 times higher than Fe/CNT-in). Different to CNT containing monometallic iron nanoparticles, the C_2-C_4 olefin selectivity and olefin to paraffin ratio decrease with increase in the iron particle size both at 10 bar

and under atmospheric pressure (**Table 4, Figure 8** and **9**). Higher, but slightly different, light olefin selectivities over the promoted iron catalysts with different particle size might be ascribed to different coverages of the iron carbide surface with the promoters. De Jong [27] also observed this effect over Na and S promoted iron catalysts with different iron carbide particle size.

More detailed information about the intrinsic activity of CNT containing encapsulated monometallic iron nanoparticles and those promoted with Bi and Pb was obtained from the TOF values. The TOF values assuming the presence of the Fe_5C_2 under the reaction conditions are presented in **Tables 3** and **4**. TOFs are plotted as a function of iron particle size for CNT containing encapsulated monometallic and promoted iron nanoparticles measured at the 10 bar and atmospheric pressure (**Figure 11**). As expected, higher TOF were obtained at higher reaction pressure. The TOF numbers for unpromoted catalysts at both high and low pressure reaction conditions increase rapidly with increase in the particle sizes up to 6 nm and stabilise for larger metal nanoparticles. These results are consistent with those for cobalt and ruthenium catalysts for which TOF increases with the particle size up to 6-8 and stabilize at larger sizes [20, 23]. Park [24] also found the similar results over iron catalysts with varying particle size from 2 nm to 12 nm in FTS. It is noteworthy that the Bi and Pb promoted iron catalysts present ~3 times (10 bar) and ~ 5 times (1 bar) higher TOF values compared with monometallic iron catalysts.

Apart from the enhancement of FT reaction rate, confinement of iron nanoparticles in CNT also improves the catalyst stability. **Figure S8, SI** shows micrographs of two

spent Bi-promoted iron catalysts and calculated respective particle size distribution. The average particle size of spent FeBi/CNT-300 is 3.9 nm, while for the FeBi/CNT-in-400 the average size after reaction is 6.5 nm. Both the FeBi/CNT-in-300 and FeBi/CNT-in-400 catalysts show very slight sintering compared with the fresh catalysts. We can conclude that confinement is also an efficient way to improve the stability of small iron carbide nanoparticles.

4. Conclusion

Encapsulation inside carbon nanotubes affects the properties of iron nanoparticles, their catalytic performance and stability in high temperature FT synthesis. The temperature of catalyst thermal treatment has a strong effect on the size of iron nanoparticles encapsulated inside CNT. Larger iron nanoparticles were obtained after treatment at higher temperature and they exhibit better reducibility. The promoters (Bi and Pb) are located in the surface of iron with close contact and the iron sintering degree is restricted by confinement in CNT.

The presence of promoters strongly influences on the catalytic performance of iron carbide nanoparticles. The specific reaction rates (TOF) were 3-5 times higher over the Bi- and Pb –promoted catalysts compared to the unpormoted counterparts. In the unpromoted iron catalysts with confined iron nanoparticles, the TOF increases with the increase in the iron nanoparticle size from 2.5 nm to 6-8 nm and then remains stable with further increase in the iron particle size, while the product selectivity is not affected by the nanoparticle size variation.

In the Bi and Pb promoted iron catalysts, the size of encapsulated iron nanoparticles affects both the activity and selectivity. The activity shows similar trend with the unpromoted iron catalysts, while the selectivity to light olefins decreases with the increase in the iron particle size. These findings shed further light on the fundamental effects of confinement on catalysis, and provide more insights into the particle size effects in iron-based FT catalysts.

Acknowledgements

The authors thank Olivier Gardoll, Laurence Burylo and Joelle Thuriot for help with TPR, XRD measurements and ICP-OES analysis. B. G. thanks the China Scholarship Council for providing him a stipend for PhD studies in France. The authors acknowledge financial support from European Union (Interreg V project PSYCHE). The authors acknowledge financial support of the French National Research Agency (Project NANO4-FUT, ANR-16-CE06-0013).

Reference:

[1] M. Janardanarao, Industrial & Engineering Chemistry Research 29 (1990) 1735-1753.

[2] K. Cheng, J. Kang, D.L. King, V. Subramanian, C. Zhou, Q. Zhang, Y. Wang, in: C. Song (Ed.), Advances in Catalysis, Academic Press, 2017, pp. 125-208.

[3] B. Gu, S. He, W. Zhou, J. Kang, K. Cheng, Q. Zhang, Y. Wang, Journal of Energy Chemistry 26 (2017) 608-615.

[4] H.M. Torres Galvis, K.P. de Jong, ACS Catalysis 3 (2013) 2130-2149.

[5] A. Steynberg, Studies in surface science and catalysis, Elsevier, 2004, pp. 1-63.

[6] S. Abelló, D. Montané, ChemSusChem 4 (2011) 1538-1556.

[7] M. Casavola, J. Hermannsdörfer, N. de Jonge, A.I. Dugulan, K.P. de Jong, Advanced Functional Materials 25 (2015) 5309-5319.

[8] H.M.T. Galvis, J.H. Bitter, C.B. Khare, M. Ruitenbeek, A.I. Dugulan, K.P. de Jong, Science 335 (2012) 835-838.

[9] A.C. Koeken, T. Galvis, M. Hirsa, T. Davidian, M. Ruitenbeek, K.P. De Jong, Angewandte Chemie International Edition 51 (2012) 7190-7193.

[10] C. Wang, L. Xu, Q. Wang, Journal of Natural Gas Chemistry 12 (2003) 10-16.

[11] Q. Chang, C. Zhang, C. Liu, Y. Wei, A.V. Cheruvathur, A.I. Dugulan, J.W. Niemantsverdriet, X. Liu, Y. He, M. Qing, L. Zheng, Y. Yun, Y. Yang, Y. Li, ACS Catalysis (2018) 3304-3316.

[12] M.E. Dry, T. Shingles, L.J. Boshoff, Journal of Catalysis 25 (1972) 99-104.

[13] J. Lu, L. Yang, B. Xu, Q. Wu, D. Zhang, S. Yuan, Y. Zhai, X. Wang, Y. Fan, Z. Hu, ACS Catalysis 4 (2014) 613-621.

[14] A. Nakhaei Pour, M.R. Housaindokht, M. Irani, S.M. Kamali Shahri, Fuel 116 (2014) 787-793.

[15] Z.-J. Wang, S. Skiles, F. Yang, Z. Yan, D.W. Goodman, Catalysis Today 181 (2012) 75-81.

[16] V.K. Jones, L.R. Neubauer, C.H. Bartholomew, Journal of Physical Chemistry 90 (1986) 4832-4839.

[17] J. Den Breejen, P. Radstake, G. Bezemer, J. Bitter, V. Frøseth, A. Holmen, K.d. Jong, Journal of the American Chemical Society 131 (2009) 7197-7203.

[18] J.-Y. Park, Y.-J. Lee, P.R. Karandikar, K.-W. Jun, K.-S. Ha, H.-G. Park, Applied Catalysis A: General 411-412 (2012) 15-23.

[19] G. Prieto, A. Martínez, P. Concepción, R. Moreno-Tost, Journal of Catalysis 266 (2009) 129-144.

[20] G.L. Bezemer, J.H. Bitter, H.P. Kuipers, H. Oosterbeek, J.E. Holewijn, X. Xu, F. Kapteijn, A.J. van Dillen, K.P. de Jong, Journal of the American Chemical Society 128 (2006) 3956-3964.

[21] J.M.G. Carballo, J. Yang, A. Holmen, S. García-Rodríguez, S. Rojas, M. Ojeda, J.L.G. Fierro, Journal of Catalysis 284 (2011) 102-108.

[22] J.L. Eslava, X. Sun, J. Gascon, F. Kapteijn, I. Rodríguez-Ramos, Catalysis Science & Technology 7 (2017) 1235-1244.

[23] J. Kang, S. Zhang, Q. Zhang, Y. Wang, Angewandte Chemie International Edition 48 (2009) 2565-2568.

[24] J.-Y. Park, Y.-J. Lee, P.K. Khanna, K.-W. Jun, J.W. Bae, Y.H. Kim, Journal of Molecular Catalysis A: Chemical 323 (2010) 84-90.

[25] K. Cheng, M. Virginie, V.V. Ordomsky, C. Cordier, P.A. Chernavskii, M.I. Ivantsov, S. Paul, Y. Wang, A.Y. Khodakov, Journal of Catalysis 328 (2015) 139-150.

[26] P.A. Chernavskii, V.I. Zaikovskii, G.V. Pankina, A.Y. Khodakov, ChemCatChem 5 (2013) 1758-1761.

[27] H.M. Torres Galvis, J.H. Bitter, T. Davidian, M. Ruitenbeek, A.I. Dugulan, K.P. de Jong, Journal of the American Chemical Society 134 (2012) 16207-16215.

[28] J. Xie, H.M. Torres Galvis, A.C. Koeken, A. Kirilin, A.I. Dugulan, M. Ruitenbeek, K.P. de Jong, ACS catalysis 6 (2016) 4017-4024.

[29] V.V. Ordomsky, Y. Luo, B. Gu, A. Carvalho, P.A. Chernavskii, K. Cheng, A.Y. Khodakov, ACS Catalysis 7 (2017) 6445-6452.

[30] B. Gu, V.V. Ordomsky, M. Bahri, O. Ersen, P.A. Chernavskii, D. Filimonov, A.Y. Khodakov, Applied Catalysis B: Environmental 234 (2018) 153-166.

[31] W. Chen, Z. Fan, L. Gu, X. Bao, C. Wang, Chemical communications 46 (2010) 3905-3907.

[32] P. Serp, E. Castillejos, ChemCatChem 2 (2010) 41-47.

[33] G. Yu, B. Sun, Y. Pei, S. Xie, S. Yan, M. Qiao, K. Fan, X. Zhang, B. Zong, Journal of the American Chemical Society 132 (2009) 935-937.

[34] W. Chen, Z. Fan, X. Pan, X. Bao, Journal of the American Chemical Society 130 (2008) 9414-9419.

[35] C. Wang, X. Pan, X. Bao, Chinese Science Bulletin 55 (2010) 1117-1119.

[36] Z. Yang, X. Pan, J. Wang, X. Bao, Catalysis Today 186 (2012) 121-127.

[37] H. Tian, X. Li, L. Zeng, J. Gong, ACS Catalysis 5 (2015) 4959-4977.

[38] L. Yu, W.-X. Li, X. Pan, X. Bao, The Journal of Physical Chemistry C 116 (2012) 16461-16466.

[39] B.D. Cullity, Addision-Wesley Publishing Company, London (1978).

[40] D.E. Mears, Industrial & Engineering Chemistry Process Design and Development 10 (1971) 541-547.

[41] P. Weisz, C. Prater, Advances in Catalysis, Elsevier, 1954, pp. 143-196.

[42] A. Primo, J. He, B. Jurca, B. Cojocaru, C. Bucur, V.I. Parvulescu, H. Garcia, Applied Catalysis B: Environmental 245 (2019) 351-359.

[43] Y.-N. Wang, Y.-Y. Xu, H.-W. Xiang, Y.-W. Li, B.-J. Zhang, Industrial & Engineering Chemistry Research 40 (2001) 4324-4335.

[44] R.M.M. Abbaslou, J. Soltan, A.K. Dalai, Applied Catalysis A: General 379 (2010) 129-134.

[45] K. Mai, T. Elder, L.H. Groom, J.J. Spivey, Catalysis Communications 65 (2015) 76-80.

[46] V. Subramanian, V.V. Ordomsky, B. Legras, K. Cheng, C. Cordier, P.A. Chernavskii, A.Y. Khodakov, Catalysis Science & Technology 6 (2016) 4953-4961.

[47] R.M.M. Abbaslou, A. Tavassoli, J. Soltan, A.K. Dalai, Applied Catalysis A: General 367 (2009) 47-52.

[48] Z. Yu, D. Chen, B. Tøtdal, A. Holmen, Catalysis today 100 (2005) 261-267.

[49] P.A. Chernavskii, A.Y. Khodakov, G.V. Pankina, J.-S. Girardon, E. Quinet, Applied Catalysis A: General 306 (2006) 108-119.

[50] P. Chernavskii, J.-A. Dalmon, N. Perov, A. Khodakov, Oil & Gas Science and Technology-Revue de l'IFP 64 (2009) 25-48.

[51] X. Pan, X. Bao, Accounts of Chemical Research 44 (2011) 553-562.

[52] J. Guan, X. Pan, X. Liu, X. Bao, Journal of Physical Chemistry C 113 (2009) 21687-21692.

Table 1. Characterization of the supports and CNT confined monometallic Fe catalysts.

Sample	S_{BET}[a] (m^2/g)	V_{tot}[b] (cm^3/g)	D_{meso}[c] (nm)	D_{metal}[d] (nm)	D_{metal}[e] (nm)	Total H_2 consumption[f] (mmol/g)	Fe content[g] (wt%)
CNT-raw	138.2	0.43	14.0				
CNT-HNO_3	230.3	0.83	14.4	-	-	-	-
Fe/CNT-in-300	205.3	0.53	10.9	-	2.8	2.40	10.9
Fe/CNT-in-350	198.7	0.51	10.6	3.8	3.9	-	10.7
Fe/CNT-in-400	192.9	0.52	10.8	6.0	6.0	1.80	10.3
Fe/CNT-in-450	188.3	0.50	11.1	7.8	7.7	-	11.3
Fe/CNT-in-500	193.6	0.51	10.8	11.2	9.9	1.60	11.1
Fe/CNT-in-600	199.9	0.53	11.2	12.7	11.4	1.52	10.7

[a] BET surface area.

[b] Single point desorption total pore volume of pores, P/P_0=0.975.

[c] The pore diameter in the mesoporous region evaluated by the BJH method.

[d] Average particle size of iron oxide by XRD.

[e] Average particle size of iron oxide by TEM.

[f] The total H_2 consumption and iron reducibility degree from TPR analysis.

[g] The Fe content from ICP-OES.

Table 2. Characterization of CNT with confined iron nanoparticles promoted with Bi or Pb.

Sample	S_{BET}[a] (m^2/g)	V_{tot}[b] (cm^3/g)	D_{meso}[c] (nm)	D_{metal}[d] (nm)	D_{metal}[e] (nm)	Total H_2 consumption[f] (mmol/g)	Fe content[g] (wt%)	Bi or Pb content[g] (wt%)
CNT	230.3	0.83	14.4	-	-	-	-	
FeBi/CNT-in-300	200.3	0.52	11.0	-	2.6	3.0	10.2	0.88
FeBi/CNT-in-350	193.7	0.52	11.2	3.9	4.1	2.83	10.8	0.84
FeBi/CNT-in-400	183.3	0.52	11.3	6.2	5.8	2.53	10.5	0.92
FeBi/CNT-in-450	173.3	0.50	10.4	8.3	7.8	2.51	11.2	0.86
FeBi/CNT-in-500	176.6	0.48	10.8	10.8	10.3	2.40	11.3	0.83
FeBi/CNT-in-600	179.9	0.45	11.2	11.9	11.7	2.12	10.9	0.87
FePb/CNT-in-300	208.2	0.51	10.7	-	2.7	2.70	10.9	0.90
FePb/CNT-in-400	187.8	0.50	10.2	5.3	5.9	2.18	10.6	0.88
FePb/CNT-in-600	180.1	0.48	10.5	11.5	11.8	1.85	11.0	0.87

[a]BET surface area.

[b] Single point desorption total pore volume of pores, P/P_0=0.975.

[c] The pore diameter in the mesoporous region evaluated by the BJH method.

[d] Average particle size of iron oxide by XRD.

[e] Average particle size of iron oxide by TEM.

[f] The total H_2 consumption and iron reducibility degree from TPR analysis.

[g] Fe, Bi, Pb content from ICP-OES.

Table 3. Catalytic performance of CNT with encapsulated iron nanoparticles with different sizes in FT synthesis (350 °C, H_2/CO = 1/1, GHSV = 17 L/g.h (10bar) or 3.4 L/g.h (1bar), TOS = 10 h)

Catalysts	Pressure (bar)	FTY 10^{-4} $mol_{CO}g_{Fe}^{-1}s^{-1}$	TOF (s^{-1})	CO conv. (%)	CO_2 sel. (%)	Hydrocarbon selectivity (%)				$C_{2-4}^{=}$/ C_{2-4}^{o}
						CH_4	$C_{2-4}^{=}$	C_{2-4}^{0}	C_5^{+}	
Fe/AC	10	0.77	0.244	7.4	28.7	36.2	27.3	22.9	13.6	1.19
Fe/CNT-out	10	1.25	0.288	12.0	29.8	33.6	32.5	19.8	14.1	1.64
Fe/CNT-in-300	10	1.90	0.132	18.3	30.0	29.2	38.2	16.5	16.1	2.32
	1	0.09	0.006	4.3	14.0	33.4	42.0	12.3	12.3	3.41
Fe/CNT-in-350	10	2.50	0.242	24.2	32.0	28.9	37.3	15.5	18.3	2.41
	1	0.12	0.012	5.6	20.0	32.5	41.6	12.1	13.8	3.44
Fe/CNT-in-400	10	3.50	0.521	33.7	40.0	28.5	35.9	15.0	19.9	2.39
	1	0.18	0.027	8.6	27.0	32.1	41.2	11.9	14.8	3.46
Fe/CNT-in-450	10	2.70	0.516	26.0	36.0	28.6	35.7	15.7	20.0	2.27
	1	0.11	0.021	5.4	18.0	31.9	40.9	11.7	15.5	3.50
Fe/CNT-in-500	10	2.80	0.614	27.0	35.0	28.4	36.1	16.0	19.5	2.26
	1	0.11	0.027	5.3	16.0	32.2	41.1	11.8	14.9	3.48
Fe/CNT-in-600	10	2.70	0.651	26.3	33.0	28.1	36.2	16.3	19.4	2.22
	1	0.11	0.031	5.2	15.0	31.5	40.1	11.6	16.8	3.46

Table 4. Catalytic performance of CNT with encapsulated iron nanoparticles with different particle size promoted with Bi and Pb in FT synthesis (350 °C, H_2/CO = 1/1, GHSV = 17 L/g.h (10bar) or 3.4 L/g.h (1bar), TOS = 10 h)

Catalysts	Pressure (bar)	FTY 10^{-4} $mol_{CO}g_{Fe}^{-1}s^{-1}$	TOF (s^{-1})	CO conv. (%)	CO_2 sel. (%)	Hydrocarbon selectivity (%)				$C_{2-4}^{=}$/ C_{2-4}^{o}
						CH_4	$C_{2-4}^{=}$	C_{2-4}^{0}	C_5^{+}	
FeBi/CNT-in-300	10	3.7	0.239	35.7	40.1	26.4	49.0	15.1	9.5	3.25
	1	0.21	0.014	10.3	14.0	28.3	64.0	6.0	1.7	10.70
FeBi/CNT-in-350	10	4.8	0.488	46.2	42.9	25.9	47.0	17.0	10.1	2.76
	1	0.37	0.038	17.6	20.0	27.6	63.2	6.5	2.7	9.72
FeBi/CNT-in-400	10	6.1	0.878	58.7	46.0	25.5	45.0	17.0	12.5	2.65
	1	0.52	0.075	25.1	31.0	27.3	62.6	6.7	3.4	9.34
FeBi/CNT-in-450	10	5.0	0.968	48.0	43.3	25.3	43.8	18.7	12.2	2.34
	1	0.43	0.083	20.6	18.0	26.8	62.0	6.9	4.3	8.99
FeBi/CNT-in-500	10	4.9	1.252	47.0	41.3	24.6	42.2	20.7	12.5	2.04
	1	0.38	0.097	18.3	16.0	26.2	61.1	7.5	5.2	8.15
FeBi/CNT-in-600	10	4.8	1.394	46.3	41.0	24.1	40.8	22.8	12.3	1.79
	1	0.36	0.104	17.2	15.0	25.4	60.1	7.9	6.6	7.61
FePb/CNT-in-300	10	4.4	0.295	42.7	40.1	25.0	44.2	19.1	11.7	2.31
	1	0.38	0.025	18.3	20.2	25.8	62.0	6.0	6.2	10.30
FePb/CNT-in-400	10	7.4	1.083	70.7	46.0	23.4	39.9	20.7	16.0	1.93
	1	0.74	0.108	35.7	36.0	25.0	59.1	8.3	7.6	7.12
FePb/CNT-in-600	10	4.9	1.406	49.3	41.0	20.1	36.5	23.5	19.9	1.55
	1	0.42	0.123	20.2	26.0	22.1	55.5	10.7	11.7	5.19

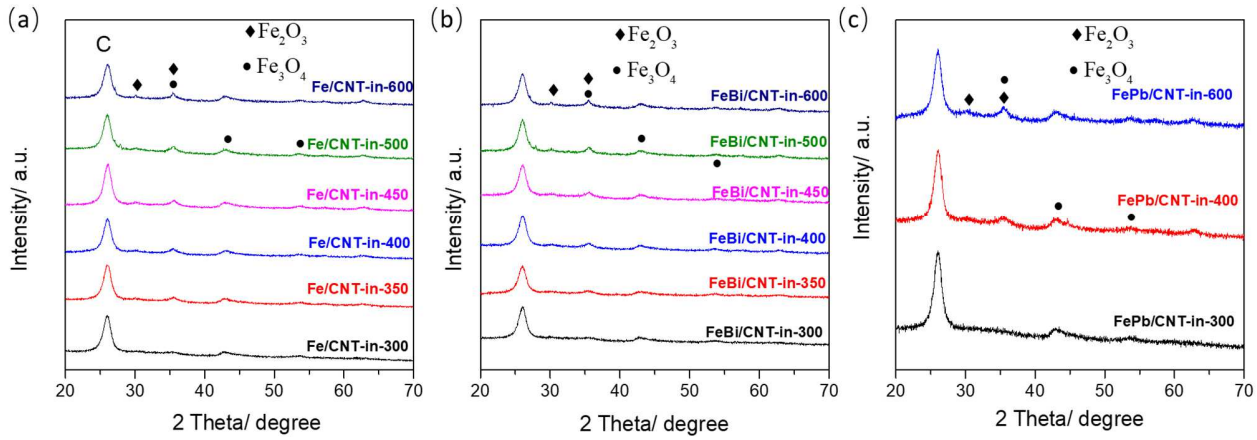


Figure 1. XRD profiles of the CNT supported iron catalysts with different calcination temperature.

(a) Fe/CNT-in, (b) FeBi/CNT-in (c) FePb/CNT-in.

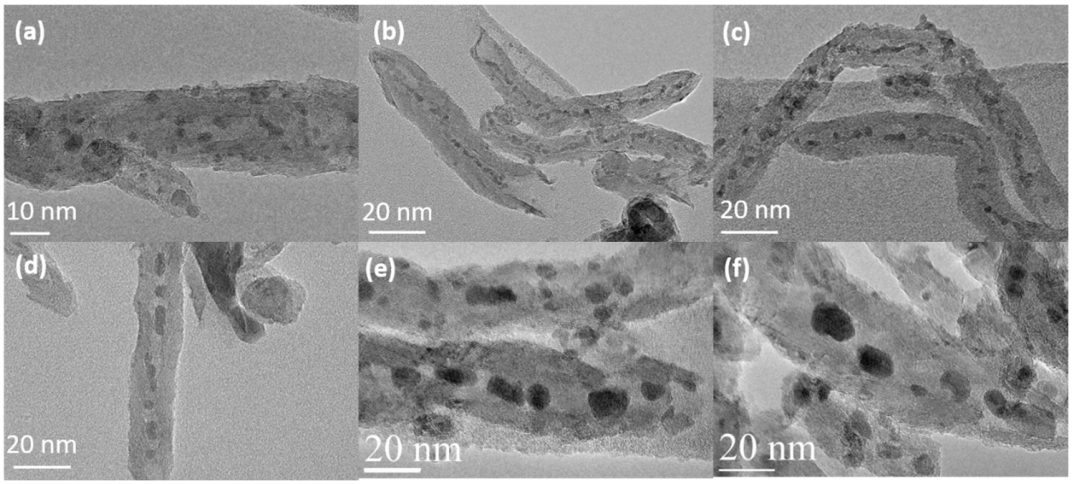


Figure 2. TEM images of the CNT confined iron catalysts under different calcination temperature. (a) Fe/CNT-in-300, (b) Fe/CNT-in-350, (c) Fe/CNT-in-400, (d) Fe/CNT-in-450, (e) Fe/CNT-in-500, (f) Fe/CNT-in-600.

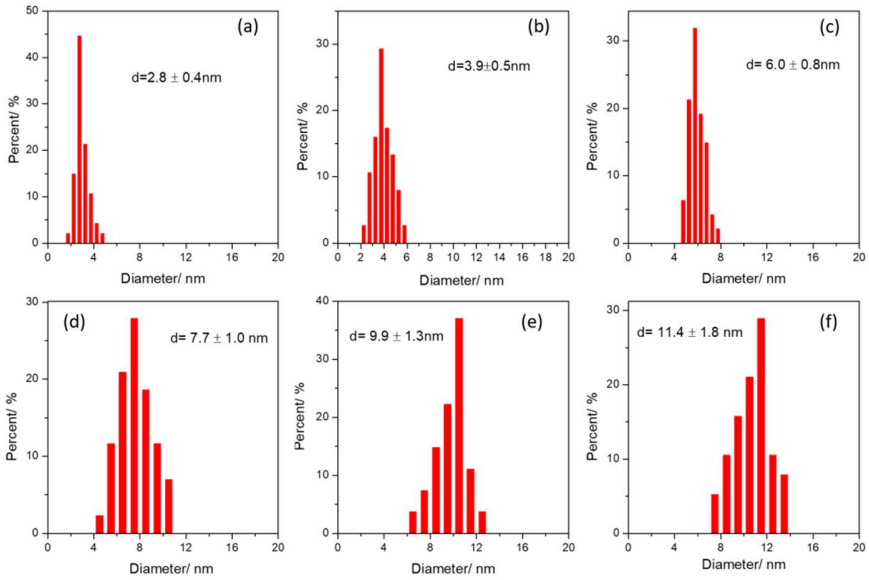


Figure 3. Particle size distribution of the CNT confined iron catalysts under different calcination temperature. (a) Fe/CNT-in-300, (b) Fe/CNT-in-350, (c) Fe/CNT-in-400, (d) Fe/CNT-in-450, (e) Fe/CNT-in-500, (f) Fe/CNT-in-600.

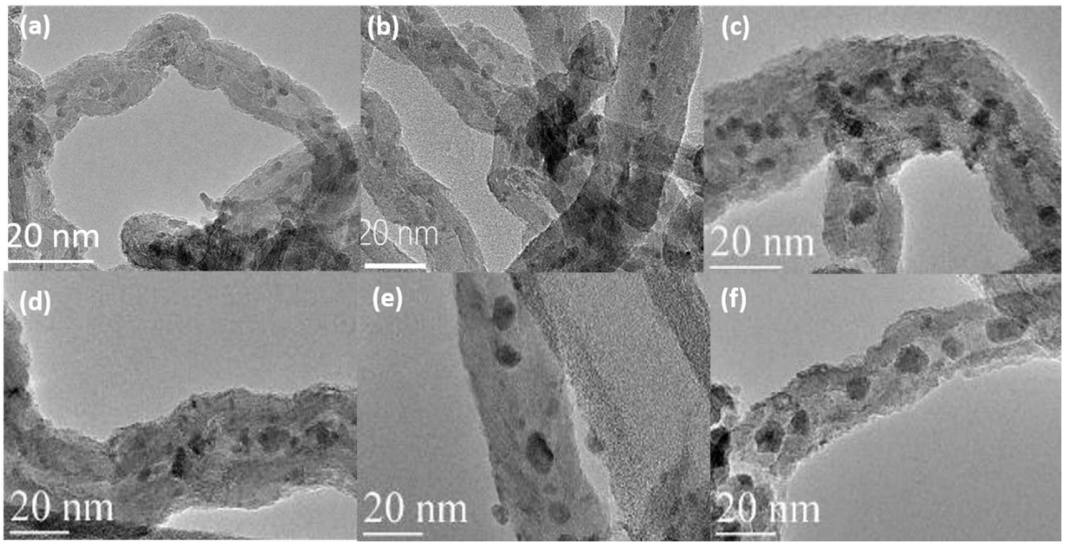


Figure 4. TEM images of the CNT confined iron catalysts promoted with Bi under different calcination temperature. (a) FeBi/CNT-in-300, (b) FeBi/CNT-in-350, (c) FeBi/CNT-in-400, (d) FeBi/CNT-in-450, (e) FeBi/CNT-in-500, (f) FeBi/CNT-in-600.

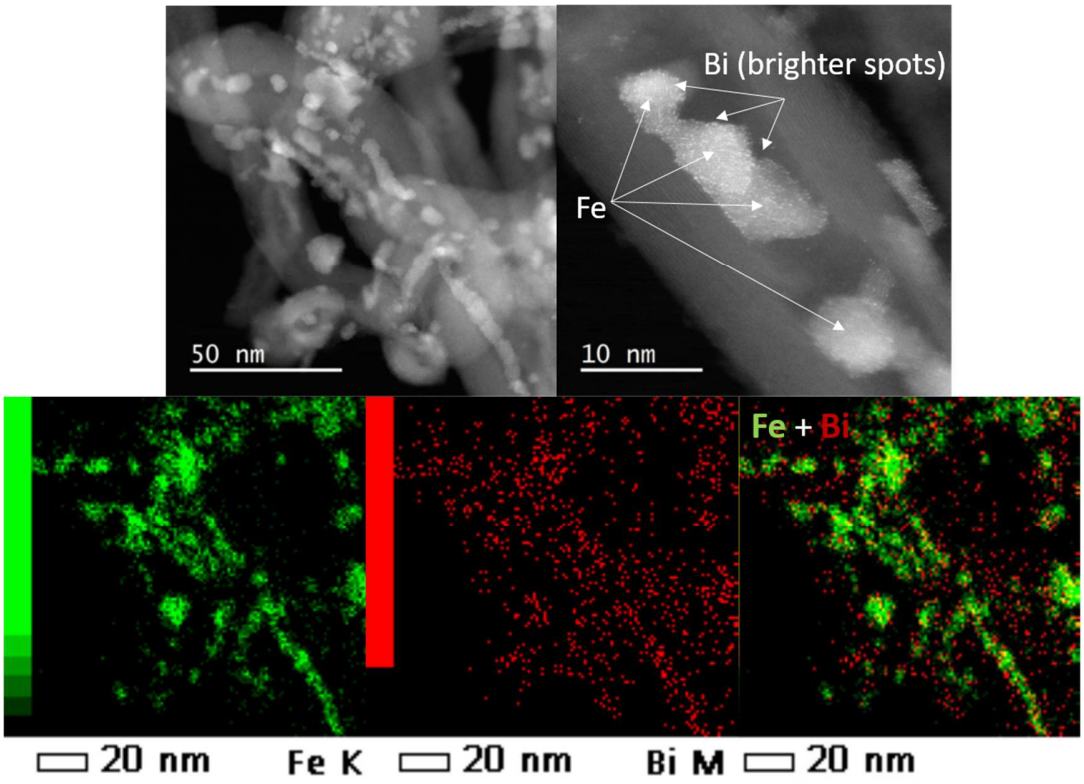


Figure 5. STEM-HAADF and STEM-EDS images for the FeBi/CNT-in-400 catalyst.

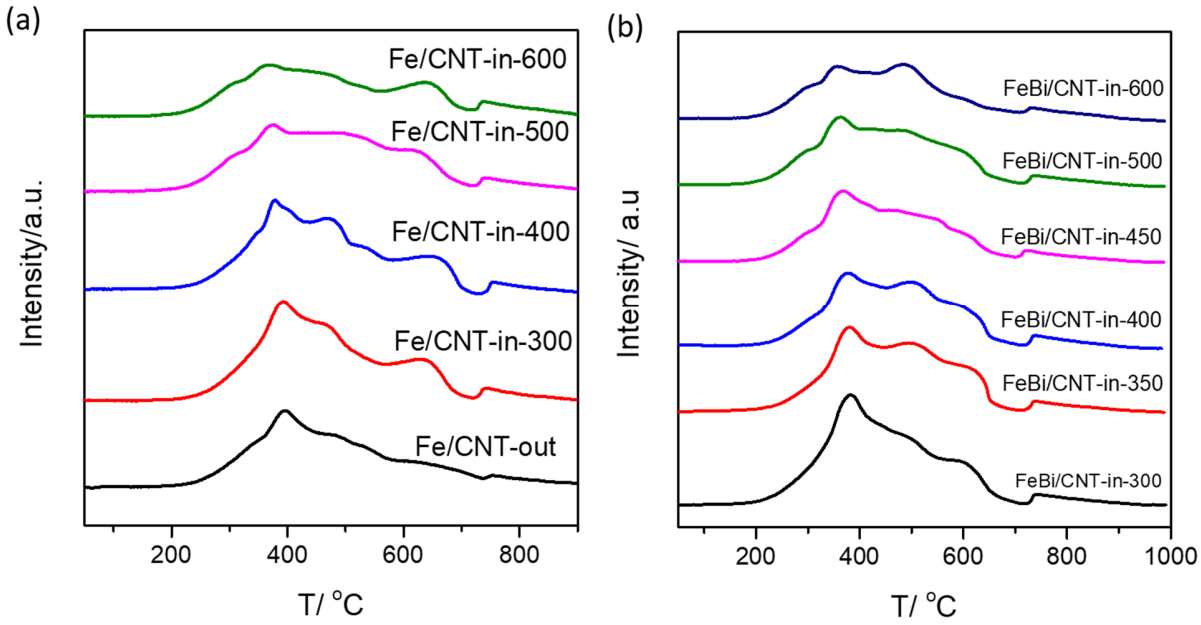


Figure 6. H_2-TPR profiles of the CNT confined iron catalysts under different calcination temperature. (a) Fe/CNT-in, (b) FeBi/CNT-in.

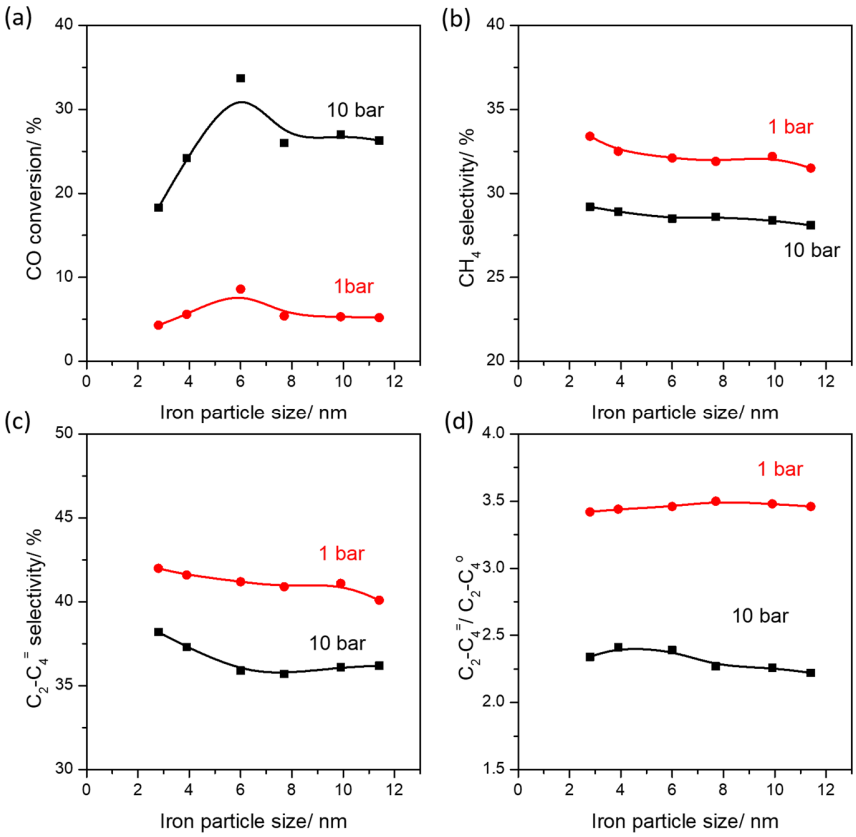


Figure 7. CO conversion and products selectivity versus iron particle size over unpromoted iron catalysts. The reaction condition: 350 °C, H_2/CO = 1/1, GHSV = 17 L/g.h, P = 1 or 10 bar, TOS = 10 h.

.

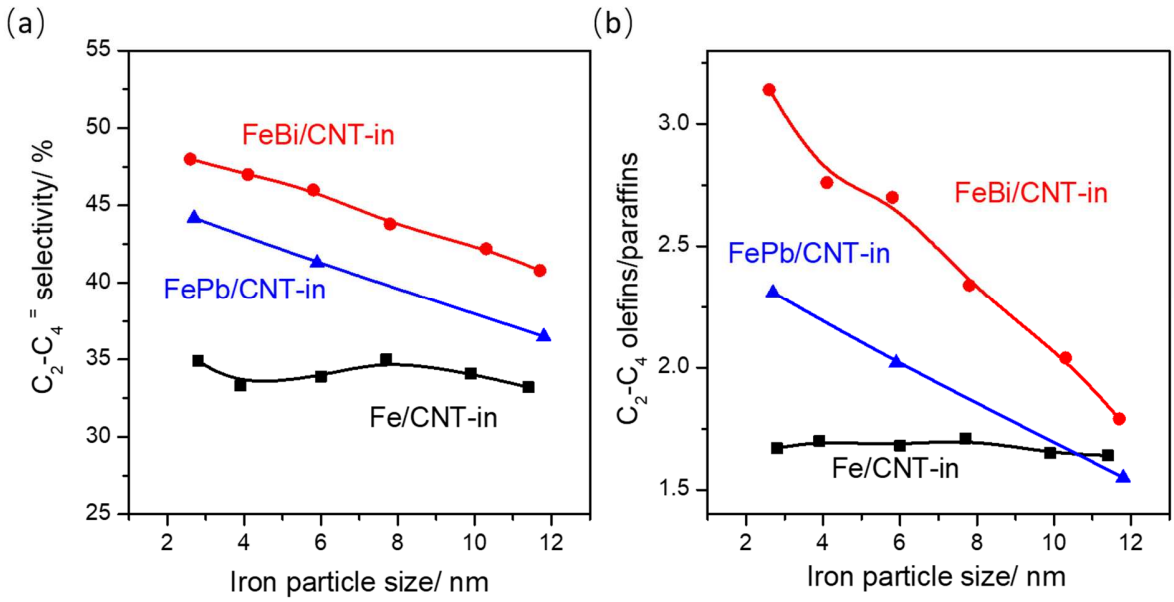


Figure 8. C_2-C_4 olefin selectivity and olefin to paraffin ratio as function of the size of iron nanoparticles confined in CNT at CO conversion of 40-50%. The reaction condition: 350 °C, H_2/CO = 1/1, GHSV = 10.2-23.8 L/g.h, P=10 bar, TOS = 10 h.

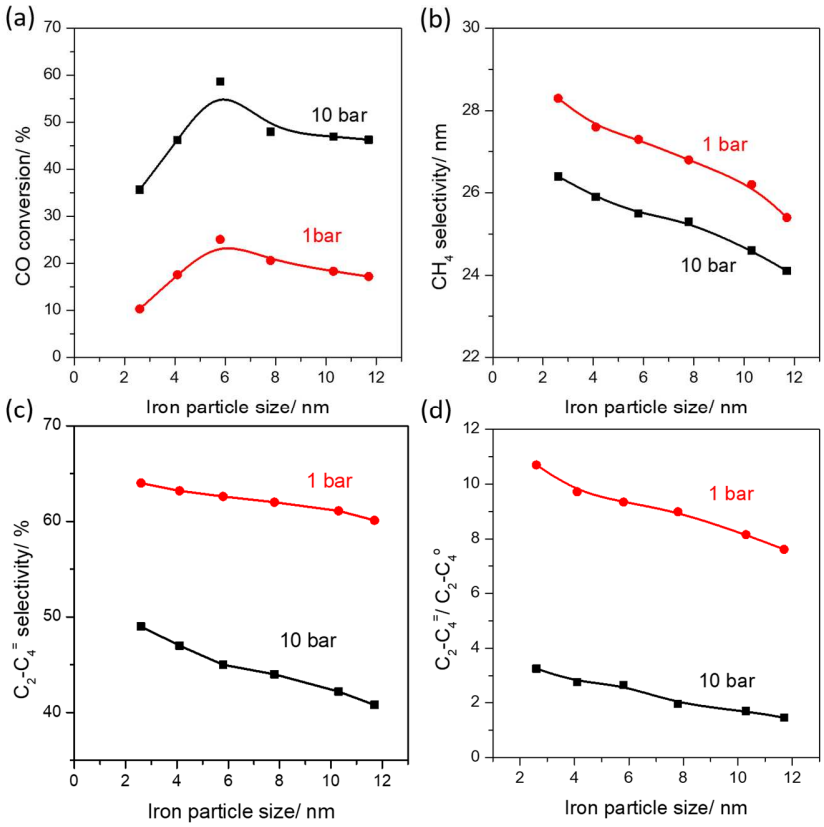


Figure 9. CO conversion and product selectivity versus iron particle size over Bi promoted iron catalysts. (350 °C, H_2/CO = 1/1, GHSV = 17 L/g.h (10bar) or 3.4 L/g.h (1bar), TOS = 10 h).

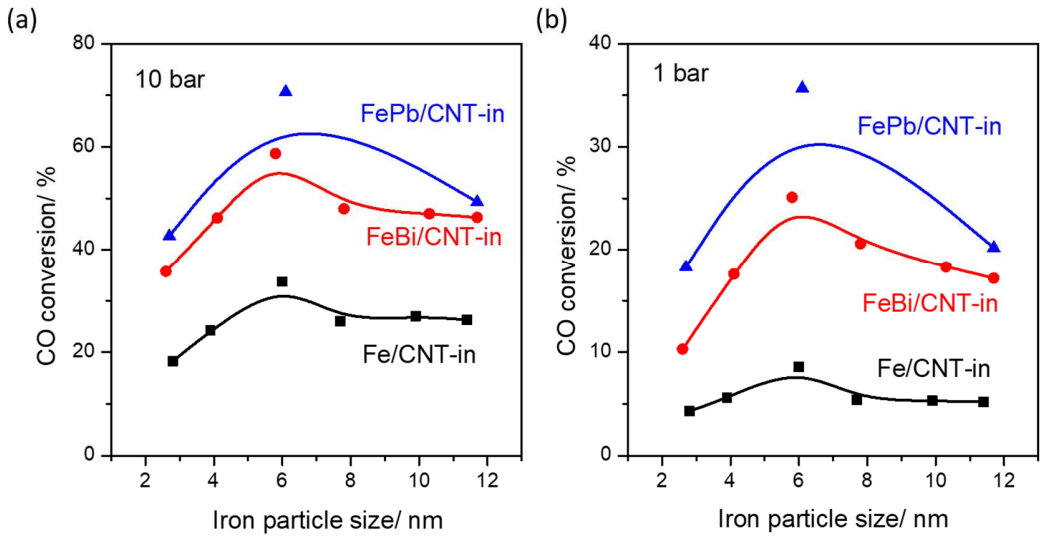


Figure 10. Iron particle size effect on the CO conversion over Bi or Pb promoted and unpromoted iron catalysts (350 ^{o}C, H_2/CO = 1/1, GHSV = 17 L/g.h (10bar) or 3.4 L/g.h (1bar), TOS = 10 h).

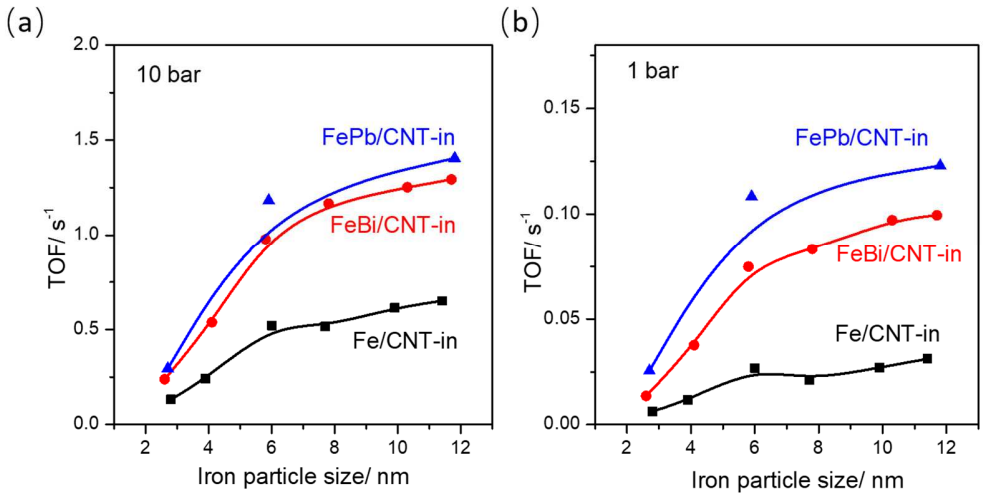
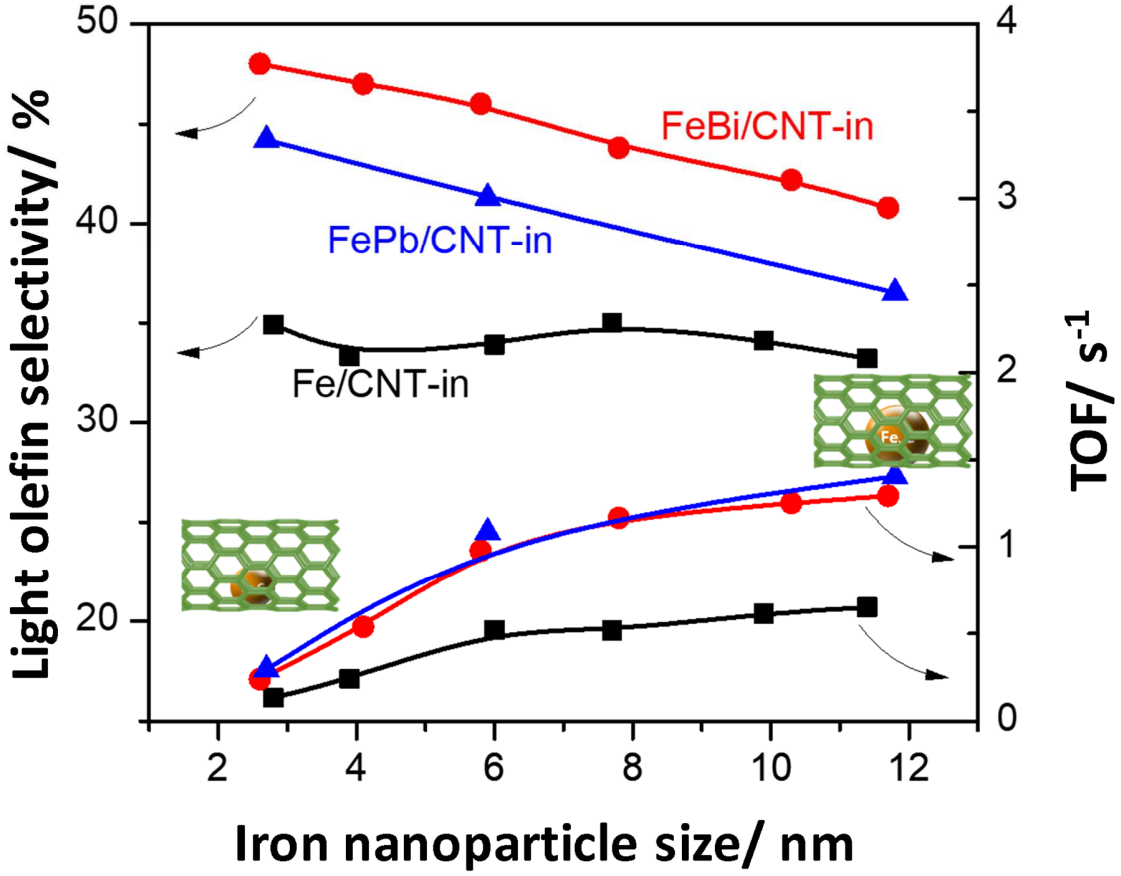


Figure 11. Iron particle size effect on the TOF (350 °C, H_2/CO = 1/1, GHSV = 17 L/g.h (10bar) or 3.4 L/g.h (1bar), TOS = 10 h).


Light olefin selectivity/ %
TOF/ s-1
Iron nanoparticle size/ nm
FeBi/CNT-in
FePb/CNT-in
Fe/CNT-in
50
40
30
20
4
3
2
1
0
2
4
6
8
10
12